Plasmon Raman scattering and photoluminescence of heavily doped *n*-type InP near the Γ-X crossover

S. Ernst, A. R. Goñi, K. Syassen, and M. Cardona
Max-Planck-Institut für Festkörperforschung, Heisenbergstrasse 1, 70569 Stuttgart, Germany
(Received 12 May 1995)

We have measured Raman scattering by coupled longitudinal-optic-phonon-plasmon modes and photoluminescence in heavily doped *n*-type InP under hydrostatic pressure and at low temperatures. The combination of both methods allows us to determine the pressure dependence of the carrier density and the enhancement of the effective electron mass of the Γ conduction-band minimum due to nonparabolicity. Above 10.3 GPa a striking change in the frequency of the upper coupled mode is observed, which is attributed to the transfer of electrons from the Γ minimum to *X*-related states. From the onset pressure for the Γ to *X* electron transfer we determine the pressure coefficient of the indirect Γ-*X* gap [−17(3) meV/GPa] and a pressure of 11.2 ± 0.4 GPa for the Γ-*X* conduction-band crossover in undoped InP.

I. INTRODUCTION

The popular use of hydrostatic pressure in the study of direct gap III-V tetrahedral semiconductors partly arises from the fact that the energy separation of the Γ_{8V} and Γ_{6C} band edge states, formed from bonding and antibonding orbitals, respectively, is very sensitive to a reduction of the lattice constant.[1,2] This allows a controlled tuning of the band structure towards a degeneracy and finally a crossover of zone center (Γ) and zone boundary (*X*) conduction-band states. The prototype example is GaAs,[3–6] with a Γ-*X* crossover at about 4.2 ± 0.2 GPa.[6]

A similar behavior is expected for InP, but shifted to higher pressures due to a larger Γ-*X* separation [about 1 eV in InP vs 0.5 eV in GaAs (Ref. 7)]. However, in InP, the expected transition from direct to indirect falls in the pressure range of the structural phase transition to the rocksalt structure near 10 GPa.[8–10] Results of transport and optical measurements have been interpreted in terms of a conduction band crossover in InP at pressures well below the phase transition [$P_c = 7$ to 8 GPa (Refs. 11–13)] or in its immediate vicinity [$P_c = 10.2-10.4$ GPa (Refs. 8, 9, and 14)]. According to more recent optical studies[15–17] the crossover does not occur below the phase transition.

In *n*-type doped semiconductors the pressure-driven approach towards a Γ-*X* crossover results in the transfer of electrons between conduction-band minima. This transfer starts at pressures *below* the actual degeneracy of band minima. The electron transfer manifests itself in the optical response of the free carriers. The plasmon frequency ω_p in heavily *n*-doped ($n \geqslant 5\times10^{17}$ cm^{-3}) direct gap semiconductors is comparable to the optical-phonon frequencies, ω_{TO} and ω_{LO}. Due to the polar character of the zinc-blende lattice, the longitudinal-optical (LO) phonon interacts with the macroscopic electric field of the plasmon giving rise to the formation of coupled L_+ and L_- modes. These frequencies are given by the coupled mode equation[18]

$$\omega_{\pm}^2 = \frac{1}{2}\{(\omega_p^2+\omega_{\mathrm{LO}}^2) \pm [(\omega_p^2-\omega_{\mathrm{LO}}^2)^2 + 4\omega_p^2(\omega_{\mathrm{LO}}^2+\omega_{\mathrm{TO}}^2)]^{1/2}\}. \quad (1)$$

The coupled mode frequencies depend strongly on the free carrier density (see Fig. 1). For high carrier densities the upper mode (L_+) behaves plasmonlike, the lower mode (L_-) shows a phononlike behavior. The plasmonlike mode is the one which should be sensitive to the onset of electron transfer upon approaching a Γ-*X* band crossing.

We have investigated the effect of hydrostatic pressure on the coupled LO-phonon-plasmon modes in heavily doped *n*-InP, using Raman scattering at low temperatures. Raman measurements have been combined with photoluminescence (PL) studies in order to determine the pressure dependence of the Fermi energy and the renormalized direct gap energy. The Raman line shape is analyzed in terms of the Lindhard-Mermin dielectric function,[19,20] which takes into account the effects of spatial dispersion and finite linewidths. Using the results of both PL and Raman measurements, we have determined the effective mass and the charge density as a function of hydrostatic pressure. We find a significant decrease of the carrier density to start near 10.3 GPa. This reversible behavior is interpreted as a precursor effect of the Γ-*X* transition in InP.

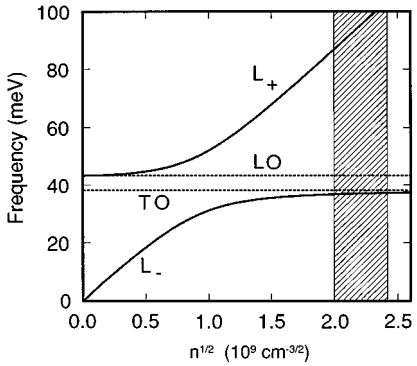

FIG. 1. Energies of the coupled L_- and L_+ modes as a function of charge density. The energies of the modes are calculated from the coupled-mode equation. Parameters corresponding to InP were used in the calculation.

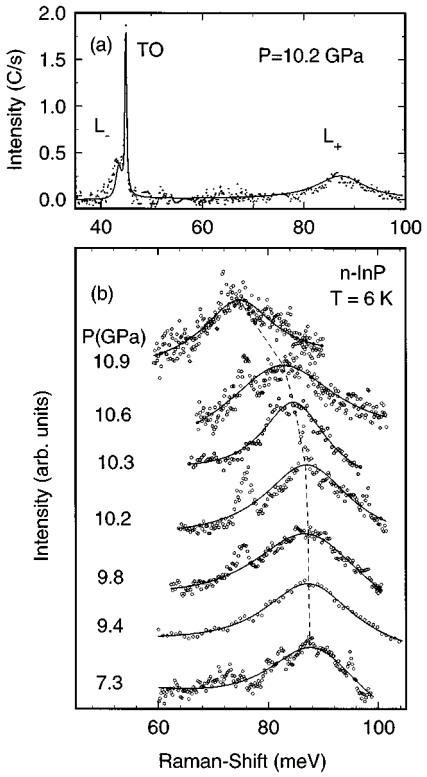

FIG. 2. (a) Raman spectrum of n-doped InP at 10.2 GPa showing the L_+ and L_- modes as well as the TO phonon. The solid line represents the result of a fit using Eq. (3) and an additional Lorentian for the TO phonon. (b) The L_+ mode of InP for different pressures. The pressure-induced shift of the L_+ mode can be seen clearly above 10.2 GPa. The peak at about 70 meV is spurious luminescence.

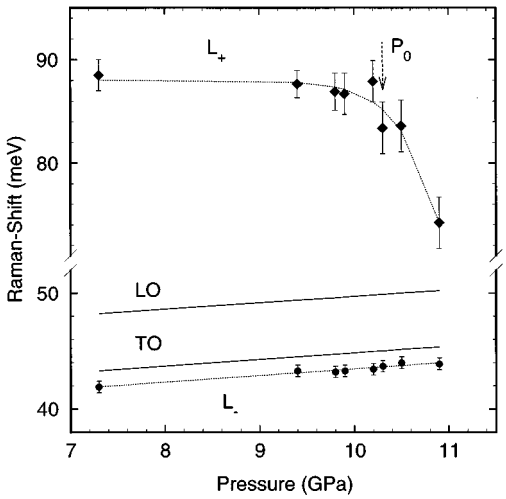

FIG. 3. Pressure dependence of the frequency of the L_+ and L_- modes. The L_+ mode shows a strong dependence on the charge density (plasmonlike behavior), the L_- mode behaves like a phonon.

II. EXPERIMENTAL DETAILS

The (100)-oriented InP single crystal sample was n-doped with sulfur having a nominal carrier concentration of 5.9×10^{18} cm^{-3}. The samples were mechanically polished down to thicknesses of approximately 30 μm. The surface was cleaned by chemical etching with a $1HCl{:}2H_2SO_4{:}3HNO_3$ etch.[21] High pressure PL and inelastic light scattering experiments were performed in a gasketed diamond anvil cell at low temperature (6 K). Condensed helium served as a pressure transmitting medium in order to ensure fully hydrostatic conditions. The pressure was measured to within ±0.03 GPa by using the standard ruby luminescence method[22–24] with temperature correction of the calibration according to Ref. 25. Raman spectra were measured only at pressures above 6 GPa, where the fundamental band gap has increased sufficiently to allow for below-gap excitation, using the 799.3 nm line of a Kr^+ ion laser (laser spot size of 30 μm). The scattered light (backscattering geometry) was dispersed by a Jobin-Yvon T64000 triple monochromator and measured by multichannel detection using a CCD (charge coupled device).

III. RESULTS AND DISCUSSION

A. Raman and photoluminesence spectra

Figure 2(a) shows a representative Raman spectrum of n-InP for $P=10.2$ GPa. In addition to the L_+ and L_- coupled LO-phonon-plasmon modes of the bulk, the spectrum shows the unscreened TO phonon from the surface depletion region.[26] In Fig. 2(b), the L_+ mode spectrum is plotted for several pressures. Below $P=10.3$ GPa the frequency of the L_+ mode remains almost constant. For higher pressures this plasmon shifts to lower energy. Finally, an increase of the applied pressure from 10.9 GPa to 11.0 GPa induces the structural phase transition into the rocksalt high pressure phase. As a consequence, Raman modes are not observed any more.

Figure 3 shows the frequencies of the coupled modes for heavily doped InP at pressures up to 11.0 ± 0.1 GPa, as obtained from a Lorentian line shape fit of the Raman spectra. Up to 10.2 GPa the L_+-mode frequency remains nearly constant. The onset for the decrease in frequency of the L_+-mode is observed at $P_c=10.3$ GPa. No change in the frequency of the L_- is observable. This is related to the plasmonlike behavior of the L_+-mode at these high carrier densities, which implies that the L_- mode behaves basically phononlike. The decrease of the L_+-mode frequency is attributed to a reduction of the free carrier density, which is taken as evidence for electron transfer between conduction-band minima.

Since a major change of the L_+-mode frequency occurs in the vicinity of the structural phase transition, it is important to note that the Raman as well as PL data were obtained in three up-down pressure cycles: First, we have measured Raman and PL up to 10.2 GPa. Then the pressure was decreased down to 7.3 GPa. In a second cycle, we increased the pressure in steps up to 10.6 GPa and subsequently released it down to 9.8 GPa. In the third cycle, we have measured up to pressures above the phase transition. The reversible behavior rules out the possibility that the reduction in carrier density originates from defects produced in the immediate vicinity of the structural transition. Thus, we attribute the change in free carrier density to the electron transfer from the Γ minimum to X-related states.

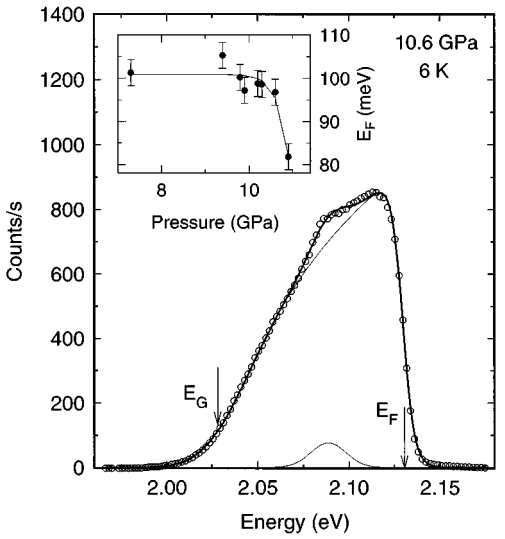

FIG. 4. Photoluminescence spectrum of n-InP at $P=10.6$ GPa (dots). Also shown is the fit of the line shape function Eq. (2) (solid line). The inset displays the Fermi energy versus the applied hydrostatic pressure.

In order to determine the carrier density from an analysis of the Raman spectra, we need additional information on the band gap energy and Fermi energy. These parameters are obtained from PL spectra. Figure 4 shows a low temperature PL spectrum for $P = 10.6$ GPa. The spectral shape is interpreted in terms of a square root density of states for the conduction band with a low energy tail characteristic of degenerate semiconductors. The high frequency cutoff of the PL spectrum corresponds to the Fermi energy E_F.

In the case of high doping, wave vector conservation breaks down.[27,28] Furthermore, dispersion of the hole states can be neglected on account of the large heavy hole mass. With these assumptions, the line shape function may be written as[29,30]

$$L(\hbar\omega)\sim f_e(\hbar\omega-E_g,E_F)\times\int_0^{\hbar\omega-E_g}\sqrt{\hbar\omega-E_g-E'}\,e^{-(E')^2}dE'. \quad (2)$$

Here, f_e is the Fermi distribution function for the degenerate electrons in the conduction band. Modification of the square root density of states, due to degeneracy of band edge and donor states, is taken into account by introducing a Gaussian broadening.

The direct band gap E_g and E_F are obtained by fitting the above line shape function to the experimental PL spectra (see solid line in Fig. 4). The additional weak line possibly originates from band to acceptor transitions.[31] Due to many-body effects doped semiconductors show a renormalization of the fundamental gap.[31] In the pressure range below 10 GPa, we find for our sample a reduction of E_g by 74 ± 15 meV compared to undoped InP. The inset to Fig. 4 displays the Fermi energy as a function of pressure. The Fermi energy stays essentially constant ($E_F=102\pm5$ meV) up to about 10 GPa and shows a sharp decrease for higher pressures.

B. Analysis of plasmon spectra

For coupled LO-phonon-plasmon modes the theoretical line shape of the Raman spectrum is given by[18]

$$L(q,\omega)\sim\left(\frac{\omega_{\mathrm{LO}}^2-\omega^2}{\omega_{\mathrm{TO}}^2-\omega^2}\right)^2\mathrm{Im}\left[-\frac{1}{\epsilon(q,\omega)}\right], \quad (3)$$

where $\epsilon(q,\omega)$ is the total dielectric function of the coupled plasmon optical-phonon system and $\mathbf{q}$ is the scattering wave vector. The frequencies ω_{TO} and ω_{LO} refer to TO and LO phonons. The electronic contribution to the longitudinal response function $\mathrm{Im}[-1/\epsilon(q,\omega)]$ is calculated using the Lindhard expression.[19] At carrier densities above 1×10^{17} cm^{-3} and $q\geqslant5\times10^5$ cm^{-1} Landau damping effects of the plasmons become important. Thus, collision damping is included in the Lindhard function in the relaxation-time approximation of Mermin.[20,32] Damping of phonons is neglected. Details about the corresponding analytical expression used for fitting experimental spectra are given in the Appendix.

The spectral function $L(q,\omega)$ depends on two parameters, the free carrier density n and the effective electron mass m^*. These parameters cannot be determined uniquely using Raman spectra only. Furthermore, they are not independent of each other. Due to the heavy doping we have to take into account the effect of band nonparabolicity arising from the filling of the conduction band up to E_F. The effective mass m^* is then given by[31]

$$\frac{m^*}{m_0}=\frac{m_0^*(P)}{m_0}\left(1-2\alpha(3\pi^2)^{2/3}\left[\frac{\hbar^2}{2m_0^*(P)}\right]\frac{n^{2/3}}{E_g(n,P)}\right)^{-1}. \quad (4)$$

Here $E_g(P)$ is the renormalized gap energy, m_0^* is the effective mass in the *undoped* material, and α the nonparabolicity factor, which includes terms up to order k^6.[33] Following the $\mathbf{k}\cdot\mathbf{p}$ theory,[34,35] we assume a linear dependence of the bottom-of-the-band effective mass parameter in the undoped case:

$$m_0^*(P)=m_0^*\frac{E_g(P)}{E_g(0)}. \quad (5)$$

Using now the values of $E_F(P)=\hbar^2(2\pi^2n(P))^{2/3}/2m^*$ and $E_g(P)$ obtained from the PL data, $L(q,\omega)$ can be fitted to the Raman spectra with basically two adjustable parameters, the free carrier density n and the collision broadening Γ. From the fits we obtain a value of about 8 meV for the broadening parameter Γ which is essentially independent on pressure. Furthermore, the pressure dependent phonon frequencies were used as fixed parameters, calculated using the Murnaghan equation and the Grueneisen relation with the mode Grueneisen parameters and zero pressure frequencies for the optical phonons.[36–38] The solid line in Fig. 2(a) corresponds to the result of a least squares fit of a model response function to the experimental spectrum.

Figure 5(a) shows the carrier density as a function of pressure. The charge density n remains nearly constant up to 10.2 GPa. Above this pressure n decreases from 5.8×10^{18} cm^{-3} to 4.0×10^{18} cm^{-3}. We emphasize that consistency between the PL and Raman results can be attained only if the pressure

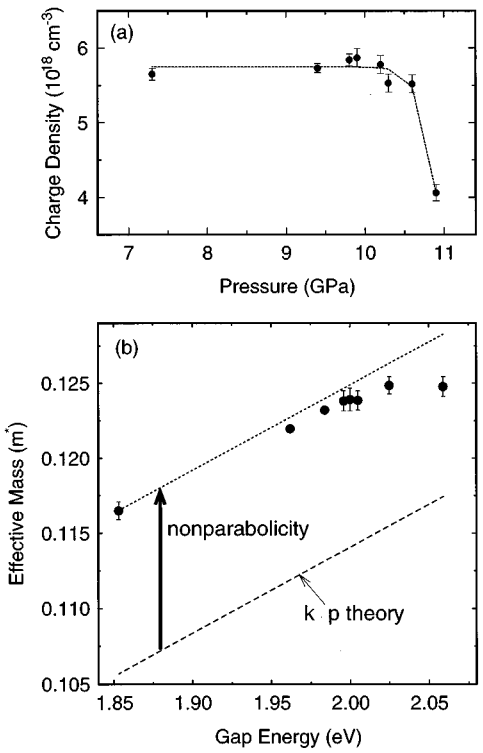

FIG. 5. (a) Charge density in n-InP as a function of pressure. We have determined the critical pressure of the Γ-X crossover from the onset of the decrease of the charge density. (b) Effective mass of n-InP as a function of gap energy. The Kane model (dashed line) predicts a linear increase with increasing gap energy. The nonparabolicity shifts the mass by a constant amount. The deviation of the experimental data from the dotted line at energies above 2 eV is attributed to a decrease in carrier density and, therefore, a reduction of the nonparabolicity.

and nonparabolicity effects on the electron effective mass are taken into account. The dashed area in Fig. 1 represents the change of the charge density in our sample due to the application of hydrostatic pressure.

In Fig. 5(b), the effective mass is plotted versus gap energy. The dashed line represents the expected variation of m_0^* within the $\mathbf{k}\cdot\mathbf{p}$ theory as given in Eq. (5). In the doped material the nonparabolicity results in a mass increase. However, the mass displays a similar linear dependence on band gap as in the undoped case. We associate the drop of the effective mass at gap energies above 2.0 eV, with a decrease in carrier density in the Γ valley and the related decrease of nonparabolicity effects.

C. Γ-X crossover in InP

The onset pressure P_0 for the decrease in frequency of the coupled modes is expected to be lower than the crossover pressure P_c because the pressure induced transfer of electrons starts when E_F at the Γ minimum and shallow states at the X point become degenerate in energy. We assume a shallow sulfur donor state as ground state in the X point, similar to our results for indirect GaAs.[39] These X-related donors are characterized by a large effective mass and a binding energy of several tenths of meV, which leads to a freeze out of carriers into these donor levels.

The energy separation between the bottom of the conduction band in Γ and the lowest states in the X-point at the onset pressure (P_0=10.3 GPa) is the sum of the Fermi energy and of the donor binding energy at the X point:

$$\Delta E = E_f + E_{b_x}. \tag{6}$$

The Fermi energy below P_0 is $E_F = 102 \pm 5$ meV, the binding energy of the sulfur donor at the X point is assumed to approximately $E_{b_x}=60\pm30$ meV. Using the literature value for the Γ-X gap energy at ambient pressure [the average value is 2.33 eV (Refs. 7, 14, and 16)], we obtain the linear pressure coefficient of

$$\frac{dE_X}{dP} = -17\pm3\ \frac{\text{meV}}{\text{GPa}} \tag{7}$$

for the X gap of InP, which is similar to that measured in $Ga_xIn_{1-x}P$ ternary compounds.[14,16]

Now, we have all the necessary information for the determination of the crossover pressure in undoped InP. Taking the effect of band gap renormalization (74 $\pm$ 15 meV) into account, the total energy difference between the Γ and X band reduces to 85$\pm$35 meV at 10.3 GPa.

Using the pressure coefficients of the direct gap [b=83(5) meV/GPa, $c=-16\times10^3$ meV^2/GPa^2] (Refs. 9 and 16) for undoped InP and the above pressure coefficient for the X band, we convert the energy difference in a pressure difference ΔP and extrapolate the pressure P_c for the Γ-X conduction-band crossover in *undoped* InP as

$$P_c = 11.2\pm0.4\ \text{GPa}.$$

Thus, the transition from direct to indirect behavior occurs directly above the structural phase transition, and for that reason it could not be observed before by spectroscopic means.

Recently, DX centers were observed to become nonresonant in InP near 8.2 GPa.[40] In our experiments, we find no evidence for a reduction of the charge density at pressures below 10 GPa. This can be explained by the fact that our experiments were performed under continuous laser excitation. Therefore, electrons in DX centers are optically excited from the deep donor levels over the emission barrier E_e [0.23–0.33 eV (Ref. 40)]. On the other hand, electrons in the Γ minimum cannot overcome the barrier at low temperatures, because the sum of Fermi energy and thermal energy, k_BT is less than half of the energy of the capture barrier.

IV. SUMMARY

We have investigated plasmon Raman scattering and photoluminescence of heavily doped n-InP under pressure. From a combined analysis of Raman and PL results, we have obtained the pressure dependence of the charge density and the nonparabolicity of the electron effective mass at the Γ point. Near the pressure of the Γ-X crossover P_c, we find a pronounced decrease in frequency of the L_+ mode, due to the transfer of electrons from the Γ to the X minimum, where the electrons become bound to X-related donors. This behavior sets in at lower pressure than P_c. The Γ-X crossover in

undoped InP occurs at $P_c = 11.2 \pm 0.4$ GPa, which is just above the structural phase transition.

ACKNOWLEDGMENTS

We are grateful to Dr. Y. C. Lu and Dr. E. Bauser for introducing us to the techniques of sample cleaning and etching. We also thank W. Dieterich and U. Engelhardt for technical support and H. Wendel for the preparation of the samples.

APPENDIX

We give here a brief account of how we have derived an *analytical* expression for the Raman line shape function.

In polar semiconductors, plasmons and LO phonons couple to form LO-phonon plasmon modes. In the framework of the random phase approximation, the dielectric function is described by

$$\epsilon(q,\omega) = \epsilon_\infty + 4\pi\chi(q,\omega) + 4\pi\chi_L(q,\omega), \tag{A1}$$

here, $\chi(q,\omega)$ describes the electronic contribution and $\chi_L(q,\omega)$ the contribution of the polar lattice:

$$4\pi\chi_L(q,\omega) = \epsilon_\infty \frac{\omega_{\mathrm{LO}}^2 - \omega_{\mathrm{TO}}^2}{\omega_{\mathrm{TO}}^2 - \omega^2}. \tag{A2}$$

The calculation of the electronic part starts from the temperature-dependent Lindhard expression[19] for the dielectric susceptibility,

$$4\pi\chi^0(q,\omega+i\Gamma) = \frac{e^2}{\pi^2 q^2}\int_0^{k_F} f(k,T) \times \left[\frac{1}{\frac{\hbar^2 q^2}{2m^*} + \frac{\hbar^2 \mathbf{q}\cdot\mathbf{k}}{m^*} - \hbar(\omega+i\Gamma)} + \frac{1}{\frac{\hbar^2 q^2}{2m^*} - \frac{\hbar^2 \mathbf{q}\cdot\mathbf{k}}{m^*} + \hbar(\omega+i\Gamma)} \right] \mathbf{d}^3\mathbf{k}. \tag{A3}$$

After the formal integration of Eq. (A3) for $T = 0K$, we achieve the following analytical expression for the dielectric function:

$$4\pi\chi^0(q,\omega+i\Gamma) = \frac{m^* k_F e^2}{\hbar^2 \pi q^2}\left[2 + \left\{ \frac{k_F}{q} - \frac{m^{*2}}{\hbar^2 q^3 k_F}(\omega_q - \omega - i\Gamma)^2 \right\} \ln\frac{\omega_+ - \omega - i\Gamma}{\omega_- - \omega - i\Gamma} + \left\{ \frac{k_F}{q} - \frac{m^{*2}}{\hbar^2 q^3 k_F}(\omega_q + \omega + i\Gamma)^2 \right\} \ln\frac{\omega_+ + \omega + i\Gamma}{\omega_- + \omega + i\Gamma} \right] \tag{A4}$$

with

$$\omega_\pm = \frac{\hbar q^2}{2m^*} \pm \frac{q\hbar k_F}{m^*}; \quad \omega_q = \frac{\hbar q^2}{2m^*}. \tag{A5}$$

The splitting in real and imaginary part gives:

$$4\pi\ \mathrm{Re}\,[\chi^0(q,\omega+i\Gamma)] = \frac{m^* k_F e^2}{\hbar^2 \pi q^2}\left[2 + \frac{k_F}{2q}\left\{ \ln\frac{(\omega_+ - \omega)^2 + \Gamma^2}{(\omega_- - \omega)^2 + \Gamma^2} + \ln\frac{(\omega_+ + \omega)^2 + \Gamma^2}{(\omega_- + \omega)^2 + \Gamma^2} \right\} - \frac{m^{*2}}{\hbar^2 q^3 k_F}\left(\frac{1}{2}\{(\omega_q - \omega)^2 - \Gamma^2\} \ln\frac{(\omega_+ - \omega)^2 + \Gamma^2}{(\omega_- - \omega)^2 + \Gamma^2} + \frac{1}{2}\{(\omega_q + \omega)^2 - \Gamma^2\} \ln\frac{(\omega_+ + \omega)^2 + \Gamma^2}{(\omega_- + \omega)^2 + \Gamma^2} + 2\Gamma(\omega_q - \omega)[\theta_+ - \theta_-] - 2\Gamma(\omega_q + \omega)[\delta_+ - \delta_-] \right) \right] \tag{A6}$$

and

$$4\pi\ \mathrm{Im}[\chi^0(q,\omega+i\Gamma)] = \frac{m^* k_F e^2}{\hbar^2 \pi q^2}\left[\frac{k_F}{q}(\theta_+ - \theta_- + \delta_+ - \delta_-) - \frac{m^{*2}}{\hbar^2 q^3 k_F}\left(-\Gamma(\omega_q - \omega) \ln\frac{(\omega_+ - \omega)^2 + \Gamma^2}{(\omega_- - \omega)^2 + \Gamma^2} + \Gamma(\omega_q + \omega) \ln\frac{(\omega_+ + \omega)^2 + \Gamma^2}{(\omega_- + \omega)^2 + \Gamma^2} + [(\omega_q - \omega)^2 - \Gamma^2](\theta_+ - \theta_-) + [(\omega_q + \omega)^2 - \Gamma^2](\delta_+ - \delta_-) \right) \right], \tag{A7}$$

where

$$\theta_{\pm} = -\,\mathrm{sign}(\omega_{\pm}-\omega)\,\mathrm{atan}\left[\frac{\Gamma}{|\omega_{\pm}-\omega|}\right] - \frac{\pi}{2}[1-\mathrm{sign}(\omega_{\pm}-\omega)] \tag{A8}$$

and

$$\delta_{\pm} = \mathrm{sign}(\omega_{\pm}+\omega)\,\mathrm{atan}\left[\frac{\Gamma}{|\omega_{\pm}+\omega|}\right] + \frac{\pi}{2}[1-\mathrm{sign}(\omega_{\pm}+\omega)]. \tag{A9}$$

For including collision broadening into the Lindhard expression, it is not correct to replace ω by $\omega + i\Gamma$. Such a procedure fails to conserve the local electron number. Mermin used a relaxation time approximation in which the collisions relax the electron density matrix to a local equilibrium density matrix.[20] This results in the Lindhard-Mermin function

$$\chi(q,\omega+i\Gamma) = \frac{\chi^0(q,0)(\omega+i\Gamma)[\chi^0(q,\omega+i\Gamma)]}{\omega\chi^0(q,0)+i\Gamma[\chi^0(q,\omega+i\Gamma)]}. \tag{A10}$$

By splitting Eq. (A10) into real and imaginary parts and using Eqs. (A6) and (A7), we can calculate the line shape function as

$$L(q,\omega) = \frac{1}{(1-e^{-\hbar\omega/k_BT})}\left[\frac{\omega_0^2-\omega^2}{\omega_{\mathrm{TO}}^2-\omega^2}\right]^2 \mathrm{Im}\left[-\frac{1}{\epsilon(q,\omega)}\right], \tag{A11}$$

with

$$\mathrm{Im}\left[-\frac{1}{\epsilon(q,\omega)}\right] = \frac{(\omega_{\mathrm{TO}}^2-\omega^2)^2[\mathrm{Im}\{4\pi\chi(q,\omega)\}]}{\epsilon_\infty^2 F^2(q,\omega)+(\omega_{\mathrm{TO}}^2-\omega^2)^2[\mathrm{Im}\{4\pi\chi(q,\omega)\}]^2} \tag{A12}$$

and

$$F(q,\omega) = (\omega_{\mathrm{LO}}^2-\omega^2) + \frac{1}{\epsilon_\infty}(\omega_{\mathrm{TO}}^2-\omega^2)\mathrm{Re}\{4\pi\chi(q,\omega)\}. \tag{A13}$$

[1] D. L. Camphausen, G. A. N. Connel, and W. Paul, Phys. Rev. Lett. **26**, 184 (1971), and references therein.

[2] W. A. Harrison, *Electronic Structure and the Properties of Solids* (Freeman, San Francisco, 1980).

[3] B. Welber, M. Cardona, C. K. Kim, and S. Rodriguez, Phys. Rev. B **12**, 5729 (1975).

[4] D. J. Wolford and J. A. Bradley, Solid State Commun. **53**, 1069 (1985).

[5] M. Leroux, G. Pelous, F. Raymond, and C. Verie, Appl. Phys. Lett. **46**, 288 (1985).

[6] A. R. Goñi, K. Strössner, K. Syassen, and M. Cardona, Phys. Rev. B **36**, 1581 (1987).

[7] A. Onton, R. J. Chiotka, and Y. Yacoby, *Proceedings of the 11th International Conference on Physics of Semiconductors* (Polish Scientific, Warsaw, 1972), p. 1023.

[8] I. Gorczyca, N. E. Christensen, and M. Alouani, Phys. Rev. B **39**, 7705 (1989).

[9] H. Müller, R. Trommer, M. Cardona, and P. Vogl, Phys. Rev. B **21**, 4879 (1980).

[10] C. S. Menoni and I. L. Spain, Phys. Rev. B **35**, 7520 (1987).

[11] G. D. Pitt, J. Phys. C **6**, 1586 (1973); Solid State Commun. **8**, 1119 (1970).

[12] T. Kobayashi, T. Tei, K. Aoki, K. Yamamoto, and K. Abe, J. Lumin. **24-25**, 347 (1981).

[13] T. Kobayashi, K. Aoki, and K. Yamamoto, Physica **139-140B**, 537 (1986).

[14] A. R. Goñi, K. Syassen, K. Strössner, and M. Cardona, Phys. Rev. B **39**, 3178 (1989).

[15] S. W. Tozer, D. J. Wolford, and J. A. Bradley, Bull. Am. Phys. Soc. **33**, 794 (1988).

[16] S. W. Tozer, D. J. Wolford, J. A. Bradley, D. Bour, and G. B. Stringfellow, in *Proceedings of the 19th International Conference on the Physics of Semiconductors, 1988*, edited by W. Zawadski (Polish Academy of Sciences, Warsaw, 1988), p. 881.

[17] M. Leroux, Semicond. Sci. Technol. **4**, 231 (1989).

[18] G. Abstreiter, M. Cardona, and A. Pinczuk, in *Light Scattering in Solids IV*, edited by M. Cardona and G. Güntherodt (Springer, Berlin, 1984), p. 5–150, and references therein.

[19] T. Lindhard, Dan. Mat. Fys. Medd. **28**, 881 (1954).

[20] N. D. Mermin, Phys. Rev. B **1**, 2362 (1970).

[21] B. Tuck and A. J. Baker, J. Mater. Sci. **58**, 1559 (1973).

[22] G. J. Piermarini, S. Block, J. P. Barnett, and R. A. Forman, J. Appl. Phys. **46**, 2774 (1975).

[23] H. K. Mao and P. M. Bell, Science **200**, 1145 (1978).

[24] H. K. Mao, J. Xu, and P. M. Bell, J. Geophys. Res. **91**, 4673 (1986).

[25] S. Buchsbaum, R. L. Mills, and D. Schiferl, J. Phys. Chem. **88**, 2522 (1984).

[26] The observed strong unscreened TO signal is explained for below-gap excitation as due to substantial amount of *forward* scattering by reflections at the sample back surface.

[27] V. A. Vilkotskii, D. S. Domansvskii, R. D. Kakanov, V. V. Krasovaskii, and V. D. Tkarchev, Phys. Status Solidi B **91**, 71 (1979).

[28] S. Bendapudi and D. N. Bose, Appl. Phys. Lett. **42**, 287 (1982).

[29] E. O. Kane, Phys. Rev. **131**, 79 (1963).

[30] H. C. Casey and M. B. Panish, *Heterostructure Lasers. I. Fundamental Principles* (Academic, New York 1987), p. 133ff.

[31] M. Bugajski and W. Lewandowski, J. Appl. Phys. **57**, 521 (1985).

[32] G. Abstreiter, R. Trommer, M. Cardona, and A. Pinczuk, Solid State Commun. **30**, 703 (1979).

[33] A. Raymond, J. L. Robert, and C. Bernard, J. Phys. C **12**, 2289 (1979).

[34] E. O. Kane, J. Phys. Chem. Solids **1**, 249 (1957).

[35] M. Cardona, J. Phys. Chem. Solids **24**, 1543 (1963).

[36] F. D. Murnaghan, Proc. Natl. Acad. Sci. U.S.A. **30**, 244 (1944).

[37] B. A. Weinstein and R. Zallen, in *Light Scattering in Solids IV*, edited by M. Cardona and G. Güntherodt (Springer, Berlin, 1984), p. 463–527.

[38] For experimental values, see, *Physics of Group IV Elements and III-V Compounds*, edited by O. Madelung, M. Schulz, and H. Weiss, Landolt Börnstein, New Series, Group III, Vol. 17, Pt. a (Springer-Verlag, Berlin, 1982); *Intrinsic Properties of Group IV Elements and III-V, II-IV, and I-VII Compounds*, edited by O. Madelung and M. Schulz, Landolt Börnstein, New Series, Group III, Vol. 22, Pt. a (Springer-Verlag, Berlin, 1987), and references therein.

[39] S. Ernst, A. R. Goñi, K. Syassen, and M. Cardona, J. Phys. Chem. Solids **56**, 567 (1995).

[40] J. A. Wolk, W. Walukiewicz, M. L. T. Thewalt, and E. E. Haller, Phys. Rev. Lett. **68**, 3619 (1992).